Separation Science and Technology
Publication details, including instructions for authors and subscription information:
http://www.informaworld.com/smpp/title~content=t713708471

Kinetic separation of methane/carbon dioxide by molecular sieve carbons

Ambalavanan Jayaraman[a]; Andrew S. Chiao[a]; Joel Padin[a]; Ralph T. Yang[a]; Curtis L. Munson[b]
[a] Department of Chemical Engineering, University of Michigan, Ann Arbor, MI, U.S.A. [b] Chevron Research and Technology Company, Richmond, CA, U.S.A.

Online publication date: 07 October 2002

To cite this Article Jayaraman, Ambalavanan , Chiao, Andrew S. , Padin, Joel , Yang, Ralph T. and Munson, Curtis L.(2002) 'Kinetic separation of methane/carbon dioxide by molecular sieve carbons', Separation Science and Technology, 37: 11, 2505 — 2528
To link to this Article: DOI: 10.1081/SS-120004450
URL: http://dx.doi.org/10.1081/SS-120004450

SEPARATION SCIENCE AND TECHNOLOGY, 37(11), 2505–2528 (2002)

KINETIC SEPARATION OF METHANE/CARBON DIOXIDE BY MOLECULAR SIEVE CARBONS

Ambalavanan Jayaraman,[1] Andrew S. Chiao,[1] Joel Padin,[1] Ralph T. Yang,[1,*] and Curtis L. Munson[2]

[1]Department of Chemical Engineering, University of Michigan, Ann Arbor, MI 48109-2136
[2]Separations Technology, Chevron Research and Technology Company, Richmond, CA 94802-0627

ABSTRACT

The bulk separation of CH_4/CO_2 mixture by pressure swing adsorption (PSA) on two different types of carbon molecular sieves (CMS) is analyzed. The two CMS are Bergbau–Forschung (BF) CMS and Takeda 3A CMS. Two different PSA cycles are considered, differing by whether a feed step is used. For a 50/50 feed mixture, it is shown that the separation is feasible with both sorbents to produce a methane product at over 90% purity and at reasonably high product recoveries and sorbent productivities. It is shown in this work that temperature is an important factor to consider for kinetics-based separations, and that a higher temperature is favorable for CH_4/CO_2 separation on molecular sieve where diffusion is slow. At 25°C, BF CMS yields better separation because the diffusion of both CO_2 and CH_4 are slow in the Takeda 3A CMS. Increasing the temperature decreases the

*Corresponding author. Fax: 734-763-0459; E-mail: yang@umich.edu

equilibrium adsorption amounts, but increases the diffusivities. The separation results with Takeda 3A are substantially improved when the temperature is increased to 70°C, and the separation is better than that of BF CMS at 25°C. Therefore, the rate of diffusion (rather than equilibrium) is the dominating factor in kinetics-based separations. The effects of the sorbent working capacity (defined as the difference in the amounts adsorbed of the fast diffusing component between the ends of the adsorption step and the desorption step) on the separation are illustrated. For the kinetics-based separation, a high-pressure feed step is desirable while a low-pressure purge step is not desirable. The reasons are seen clearly from the bed profiles.

Key Words: Methane–carbon dioxide separation; Kinetic separation by adsorption; Pressure swing adsorption; Molecular sieve carbon

INTRODUCTION

The bulk separation of CH_4/CO_2 mixture finds commercial application in obtaining pipeline quality (over 90%) CH_4 from the landfill gases and natural gas trapped in gas reservoirs. This pipeline quality methane finds widespread use in transportation, space heating, and even electricity generation because CH_4 has lower CO_2 emission per unit of energy produced. Conventionally, this separation is done by physical or chemical absorption of CO_2 in a solvent. Newer separation techniques such as membrane permeation (1) and equilibrium-based pressure swing adsorption (PSA) separation using 5A zeolite (2) are also presently employed to effect this separation. The adsorption equilibrium data of CH_4 and CO_2 reported on activated carbon by Dreisbach et al. (3) and on zirconium pillared clays by Pereira et al. (4) show that these sorbents could also be used for equilibrium-based CH_4/CO_2 PSA separation.

The development of carbon molecular sieves (CMS) led to the introduction of kinetically controlled PSA separations. In CMS, the narrow pore size distribution results in differences in the rate of diffusional transport through the porous network. This difference is made use of in gas separations. In addition, with the development of better modeling tools and microporous sorbents, kinetic separation is being suggested as an alternative process for many gas-separation problems. The major commercial application of kinetically controlled PSA process is nitrogen production from air using CMS (5–7).

Yang (5) suggested the possibility of kinetic separation of CH_4/CO_2 mixture making use of the slower diffusional transport of CH_4 in microporous sorbents such as CMS. Kapoor and Yang (8) showed that kinetic separation of this mixture on Bergbau–Forschung (BF) CMS is superior compared to the membrane and equilibrium PSA processes. They have used a linear driving force (LDF) model with cycle time-dependent LDF mass transfer coefficients for modeling. The objective of this paper is to investigate the effectiveness of the commercially available Takeda 3A CMS for the CH_4/CO_2 separation. A theoretical comparison of the performance of BF and Takeda 3A CMS is made for kinetically controlled PSA separation of a 50–50% mixture of CH_4/CO_2 for two different PSA cycle configurations. The adsorption isotherms and uptake curves of CH_4 and CO_2 needed for PSA simulations were measured on Takeda 3A CMS.

ADSORPTION EQUILIBRIA AND DIFFUSION RATES

The low-pressure adsorption equilibrium and diffusion rate data of CH_4 and CO_2 at 70°C and the diffusion rate data of CO_2 at 25°C on Takeda 3A were measured using thermogravimetric analysis (TGA) following the procedures described by Ackley and Yang (9). The differential adsorption bed (DAB) technique was used to measure CO_2 isotherms (30 and 70°C) and uptake rates (30°C) at pressures above 1 atm. The details of the experimental technique can be found elsewhere (10).

PSA CYCLE DESCRIPTION

Two different PSA cycles are used in the simulation studies. Both are commonly used for kinetic separations. Cycle (I) is a four-step PSA cycle and the schematic diagram of Cycle (I) is shown in Fig. 1.

The major steps for Cycle (I) are:

(1) pressurization with the feed gas (from 0.2 to 4.0 bar);
(2) high-pressure adsorption, i.e., the feed step (at 4.0 bar);
(3) countercurrent blowdown (from 4.0 to 1.01 bar);
(4) countercurrent desorption/purge (from 1.01 to 0.2 bar).

Total cycle time of 140 sec with 10 sec of pressurization, 60 sec of feed, 10 sec of blowdown, and 60 sec of desorption is taken as the base case. Except Step (2), all other steps are variable pressure steps as shown in Fig. 2. In Step (4), the purge gas concentration (95% CH_4/product) and volume are changed to obtain optimum performance.

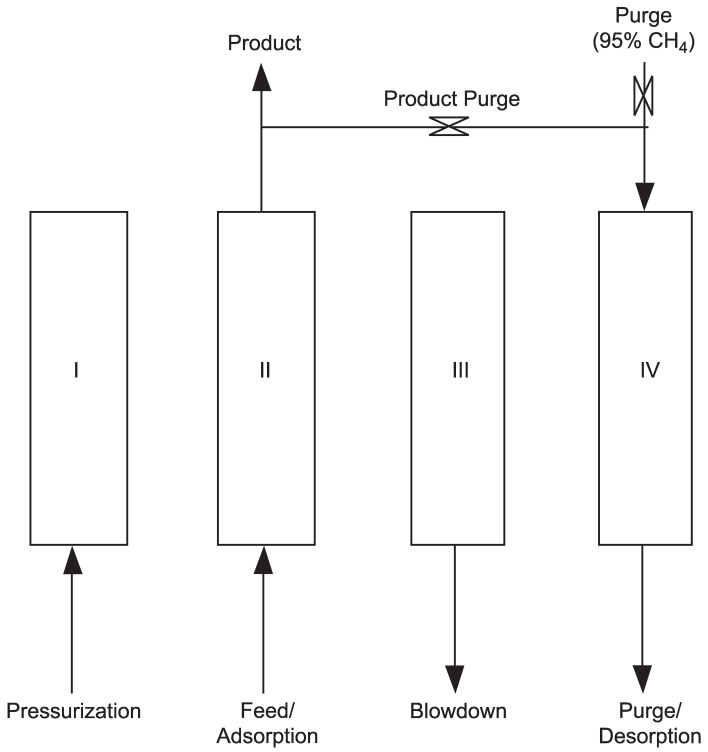

Figure 1. Steps in the four-step PSA cycle, Cycle (I), used in the simulation.

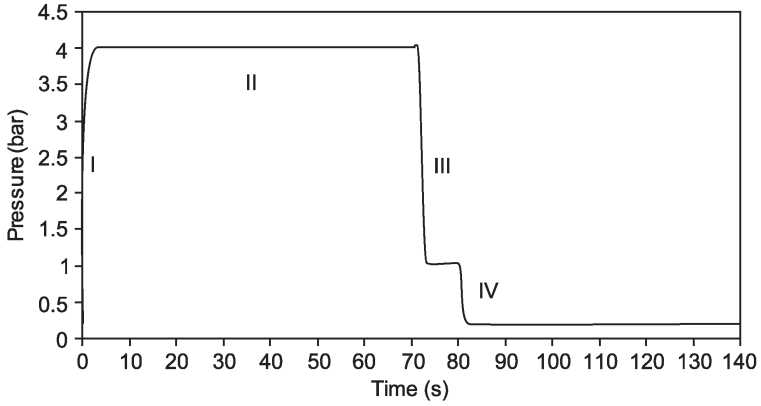

Figure 2. Typical pressure history of the adsorption column used in simulation for PSA Cycle (I).

Cycle (II) is also a four-step PSA cycle with:

(1) pressurization with feed gas (from 0.34 to 3.72 bar);
(2) cocurrent depressurization (from 3.72 to 3.36/2.60/1.29 bar);
(3) countercurrent blowdown (from 3.36/2.60/1.29 to 1.01 bar);
(4) countercurrent evacuation (from 1.01 to 0.34 bar).

All these steps were of equal time duration. A total cycle time of 240 sec and end pressures (3.36, 2.60, 1.29 bar) after the cocurrent depressurization are used to study the performance of CH_4/CO_2 PSA separation process operated in this cycle for the two sorbents under study. The detailed description of the cycle and the operating conditions are given by Kapoor and Yang (8). In Cycle (II), the outlet product velocity in the cocurrent depressurization step is varied to obtain a wider range of recoveries. The various modifications that could be made to the basic PSA cycle configurations for improving the performance have been discussed for the methane/hydrogen separation system by Doong and Yang (11). The qualitative aspects of the discussion are also valid for this system. The main thrust of this work is to investigate the suitability of the Takeda 3A CMS for CH_4/CO_2 separation and compare its performance with that of the BF CMS. The simulations were also performed for Cycle (II) on Takeda 3A CMS at 25 and 70°C and the results are compared against BF CMS at 25°C.

In order to study the performance of the two CMS under investigation, the product purity, recovery, and productivity were studied at various inlet feed velocities. In this work, the product recovery, productivity, and purge-to-feed ratio (P/F) are defined as follows:

$$\text{Product recovery} = \frac{\text{CH}_4 \text{ from Step (2)} - \text{CH}_4 \text{ used in Step (4)}}{\text{CH}_4 \text{ fed in Step (1) and Step (2)}} \tag{1}$$

$$\text{Productivity} = \frac{\text{kg CH}_4 \text{ from Step (2)} \times 3600}{\text{Total cycle time (sec)} \times \text{kg sorbent}} \tag{2}$$

$$\text{Purge-to-feed gas ratio (P/F)} = \frac{\text{Amount of CH}_4 \text{ used in Step (4)}}{\text{Amount of CH}_4 \text{ fed in Step (1) and Step (2)}} \tag{3}$$

For the cases involving purge with 95% CH_4 stream, the product recovery is not corrected to take into account the amount of CH_4 used in the purge.

MATHEMATICAL MODEL—PSA SIMULATION

The model used assumes axial dispersed plug flow of a binary gas mixture through a packed adsorbent bed with spherical adsorbent particles. The bed is

assumed to be isothermal and the external film diffusional resistance is assumed to be negligible compared to the resistance in the micropores of the sorbent. The isothermality assumption is valid due to the short cycle times as well as the low heats of adsorption (8). The axial pressure drop is neglected and gases are assumed to be ideal. The equilibrium relations for both the components are represented by extended binary Langmuir isotherms (12). The diffusional time constants are corrected for the concentration dependence by taking the value at average loading using Darken's relation (6). The exponential pressure profile (history) is assumed for the variable pressure steps with the time constant chosen according to the thumb rule described by Farooq et al. (13).

The fluid phase mass balance for component k is given by (14):

$$\varepsilon_t \frac{\partial y_k}{\partial t} - \varepsilon D_{ax} \frac{\partial^2 y_k}{\partial z^2} + \varepsilon \frac{\partial (u y_k)}{\partial z} + \frac{\rho_b RT}{P} \frac{\partial \overline{q_k}}{\partial t} + \frac{\varepsilon_t y_k}{P} \frac{dP}{dt} = 0 \tag{4}$$

The overall material balance is given by:

$$\varepsilon \frac{\partial u}{\partial z} = -\frac{\rho_b RT}{P} \sum_{k=1}^{2} \frac{\partial \overline{q_k}}{\partial t} - \frac{\varepsilon_t}{P} \frac{dP}{dt} \tag{5}$$

The particle phase mass balance for component k as given by the intraparticle diffusion equation for a sphere

$$\frac{\partial q_k}{\partial t} = \frac{D_{e,k}}{r^2} \frac{\partial}{\partial r} \left(\frac{1}{r^2} \frac{\partial q_k}{\partial r} \right) \tag{6}$$

with boundary conditions

$$\frac{\partial q_k}{\partial r} = 0 \quad \text{at} \quad r = 0 \tag{7}$$

$$-D_{e,k} \frac{\partial q_k}{\partial r}\bigg|_{r=R} = a_k \left(q_k|_{r=R} - q_k^* \right) \quad \text{at} \quad r = R \tag{8}$$

where q_k^* is the equilibrium amount adsorbed at the surface of the crystal and can be calculated using the extended binary Langmuir isotherm:

$$q_k^* = \frac{q_{mk} B_k P_k}{1 + \sum_{j=1}^{2} B_j P_j} \tag{9}$$

The volume-averaged adsorbed phase concentration $\overline{q_k}$ is given by

$$\overline{q_k} = \frac{3}{R^3} \int_0^R q_k r^2 \, dr \tag{10}$$

The boundary conditions for the fluid phase mass balance for Cycle (I) are given as follows:

(1) Pressurization step:

$$\text{at } z = 0, \quad y_k = y_{\mathrm{f},k}$$

$$\text{at } z = L, \quad u = 0$$

$$P = P(t) = P_{\mathrm{DES}} + (P_{\mathrm{H}} - P_{\mathrm{DES}})(t/\tau_{\mathrm{p}})$$

$$D_{\mathrm{ax}} \left.\frac{\partial y_k}{\partial z}\right|_{z=0} = u_{\mathrm{H}}(y_k|_{z=0} - y_{\mathrm{H},k})$$

$$\left.\frac{\partial y_k}{\partial z}\right|_{z=L} = 0 \tag{11}$$

(2) High-pressure feed step:

$$\text{at } z = 0, \quad y_k = y_{\mathrm{f},k}, \quad u = u_{\mathrm{f}}$$

$$P = P_{\mathrm{H}}$$

$$D_{\mathrm{ax}} \left.\frac{\partial y_k}{\partial z}\right|_{z=0} = u_{\mathrm{H}}(y_k|_{z=0} - y_{\mathrm{H},k})$$

$$\left.\frac{\partial y_k}{\partial z}\right|_{z=L} = 0 \tag{12}$$

(3) Countercurrent blowdown step:

$$\text{at } z = L, \quad u = 0$$

$$P = P(t) = P_{\mathrm{CBD}} + (P_{\mathrm{H}} - P_{\mathrm{CBD}})(t/\tau_{\mathrm{bd}})$$

$$\left.\frac{\partial y_k}{\partial z}\right|_{z=0} = 0$$

$$\left.\frac{\partial y_k}{\partial z}\right|_{z=L} = 0 \tag{13}$$

(4) Countercurrent desorption/purge step:

$$\text{at } z = L, \quad y_k = y_{p,k}$$

$$\text{at } z = L, \quad u = u_L$$

$$P = P(t) = P_{DES} + (P_{CBD} - P_{DES})(t/\tau_{des})$$

$$-D_{ax}\left.\frac{\partial y_k}{\partial z}\right|_{z=L} = u_L(y_{L,k} - y_L|_{z=L}), \quad u_L < 0$$

$$\left.\frac{\partial y_k}{\partial z}\right|_{z=0} = 0 \tag{14}$$

The equations for the fluid phase boundary conditions for Cycle (II) are the same as above with the only difference of an additional pressure profile equation for Step (2) and the outlet velocity being specified instead of the inlet velocity in Step (2). The above partial differential equations were solved by an implicit finite difference method using Crank–Nicolson scheme. In the simulation, 100 grid points are used in the bed with the convergence criterion set at 1×10^{-3}. The PSA simulation code developed by Sun et al. (14) in FORTRAN is used. In most simulations, the steady state was reached within 50 cycles.

RESULTS AND DISCUSSION

Equilibrium Isotherms and Uptake Rates on Takeda 3A and BF CMS

The low-pressure equilibrium data of CO_2 and CH_4 on the Takeda 3A CMS at 70°C are shown in Fig. 3. At 70°C, the Takeda 3A CMS shows a limited equilibrium selectivity for CO_2. The high-pressure CO_2 equilibrium data measured at 30 and 70°C using the DAB technique is shown in Fig. 4. The equilibrium isotherm data measured were fitted using the Langmuir equation given by:

$$q = \frac{q_m BP}{1 + BP} \tag{15}$$

The fitting parameters are listed in Table 1. The high-pressure equilibrium data for CH_4 on Takeda 3A were reported by Ma et al. (15). The BF CMS data were taken from Ref. (8) and used to plot the CO_2 and CH_4 isotherms at 25°C in Fig. 4.

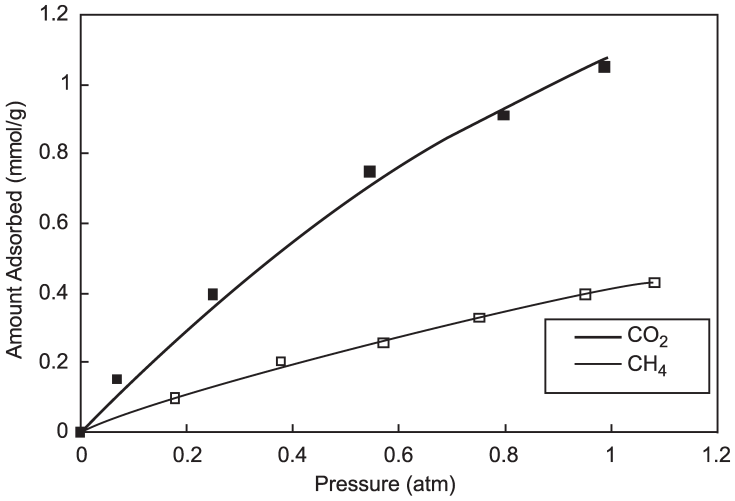

Figure 3. Equilibrium isotherms of CO_2 and CH_4 on Takeda 3A CMS at 70°C—measured in TGA.

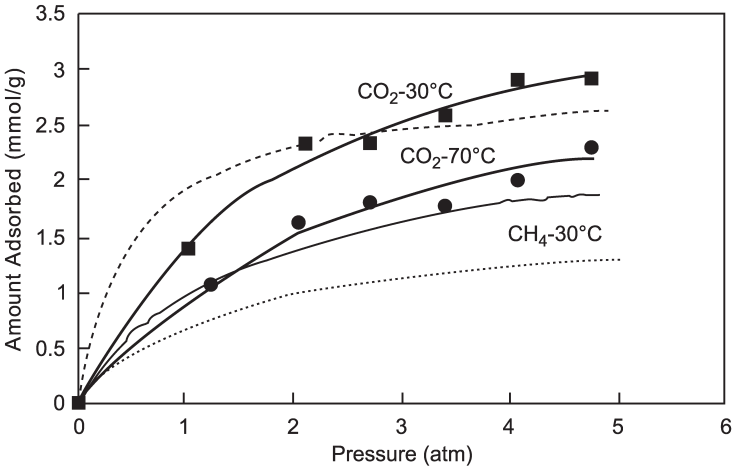

Figure 4. High-pressure equilibrium isotherms of CO_2 on Takeda 3A CMS at 30 and 70°C—measured in DAB. The isotherms of CO_2 and CH_4 on BF CMS at 25°C [taken from Ref. (8)] and CH_4 on Takeda 3A at 30°C [taken from Ref. (15)] are provided for comparison. The dashed lines represent BF CMS data and the solid lines the Takeda data.

Table 1. Values of the Langmuir Isotherm Parameters of CO_2 and CH_4 for BF and Takeda 3A CMS

Sorbent	Sorbate	T (K)	q_m (mmol/g)	B (atm^{-1})	Technique	Source
Takeda 3A CMS	CO_2	303	4.13	0.524	DAB	This work (high-pressure data)
		343	3.16	0.456		
		343	3.05	0.547	TGA	This work (low-pressure data)
	CH_4	343	1.32	0.448		
		273	3.23	0.594	Gravimetry	Ref. (15)
		323	2.01	0.844		
BF CMS	CO_2	298	2.88	1.949	—	Ref. (8)
	CH_4	298	1.76	0.607		

The fitted Langmuir parameters are summarized in Table 1, along with the values taken from the literature for both Takeda 3A and BF CMS.

The uptake rates of CO_2 at 70 and 25°C and CH_4 at 70°C on Takeda 3A CMS are measured by TGA at sub-atmospheric pressures. The uptake rate of CO_2 on Takeda 3A at a pressure of 1.5 atm and temperature of 30°C was measured using the DAB. Figure 5 shows the kinetic selectivity of CO_2 over CH_4 on Takeda 3A CMS at 70°C and BF CMS at 25°C (8). The temperature dependence of the diffusional time constant of CO_2 on Takeda 3A and the consistency between the two techniques DAB and TGA is shown in Fig. 6. The overall diffusional time constants are listed in Table 2 along with other published data for comparison. Table 3 contains the activation energy for diffusion (E) and the heat of adsorption ($-\Delta H$) for Takeda 3A CMS calculated from the data compiled in Tables 1 and 2. These activation energy and heat of adsorption data for Takeda 3A CMS are used to calculate the isotherms and diffusional time constants of CO_2 and CH_4 at 25 and 70°C for use in the PSA simulation.

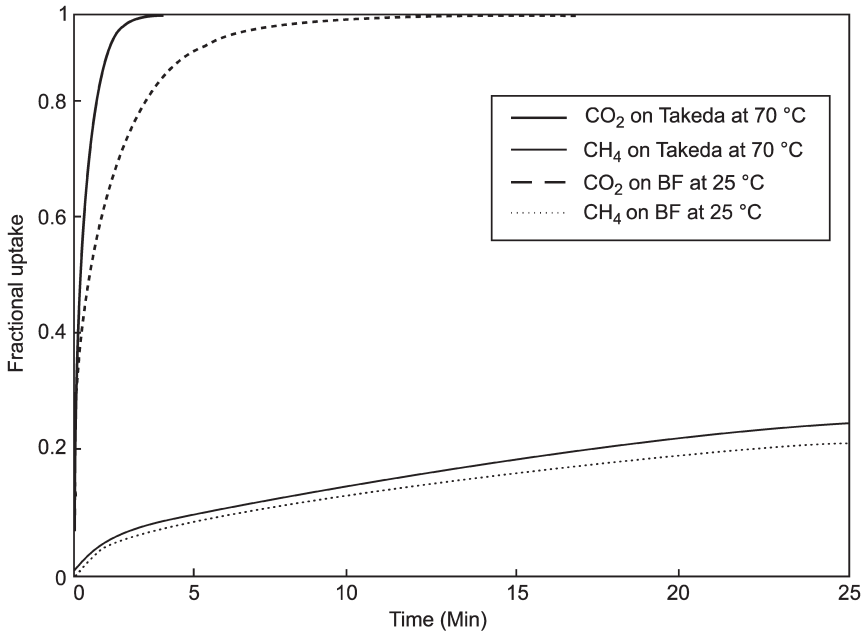

Figure 5. Uptake rates of CO_2 and CH_4 on Takeda 3A CMS at 70°C (measured by TGA) and on BF CMS at 25°C [taken from Ref. (8)] are provided for comparison.

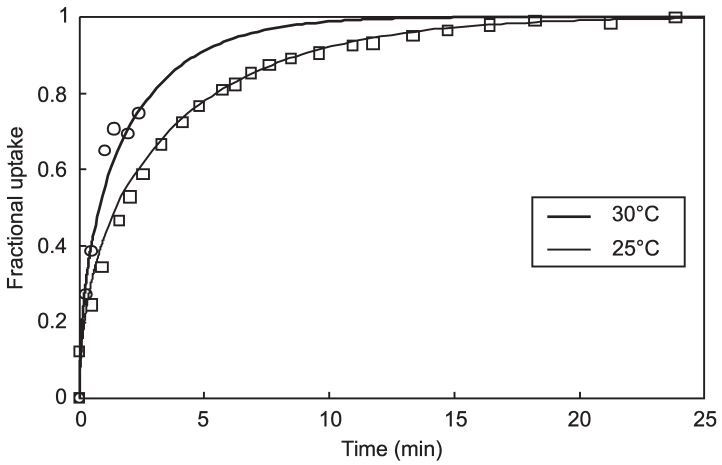

Figure 6. Uptake rates of CO_2 on Takeda 3A CMS at 30°C (measured by DAB) and 25°C (measured by TGA).

Table 2. Values of Overall Diffusional Time Constant (D_e/r^2) of CO_2 and CH_4 in BF and Takeda 3A CMS

Sorbent	Sorbate	T (K)	D_e/r^2 (sec^{-1})	Technique	Source
Takeda 3A CMS	CO_2	298	3.46×10^{-4}	TGA	This work
		303	6.52×10^{-4}	DAB	
		343	3.60×10^{-3}	TGA	
	CH_4	343	6.70×10^{-6}	Gravimetry	
BF CMS	CO_2	298	9.00×10^{-4}	Gravimetry	Ref. (8)
	CH_4	298	5.00×10^{-6}		

Table 3. Properties of Gases for Adsorption (Diffusional Activation Energy and Heat of Adsorption) on Takeda 3A CMS

Sorbate	Activation Energy, E (kcal/mol)	Heat of Adsorption, $-\Delta H$ (kcal/mol)
CO_2	9.92[a]	2.61[a]
CH_4	6.64[b]	4.06[c]

[a] Calculated using the Langmuir parameters from this work.
[b] Taken from Ref. (15).
[c] Recalculated using the Langmuir parameters from this work and Ref. (15).

PSA Simulation Results

The PSA simulations were performed for the two different PSA cycle configurations chosen. The adsorption column characteristics and specifications for Cycle (I) are listed in Table 4 and that for Cycle (II) are given in "PSA Cycle Description" and Table 8. Figure 7 shows the approach to the steady state in purity and recovery of CH_4 for a typical simulation run operating under Cycle (I).

Cycle (I)

In the current work, the cycle time/individual step times, inlet velocity, and purge-to-feed ratio are changed to study their effects on the product purity, recovery, and productivity for the two CMS sorbents under investigation. Table 5 summarizes the simulation results for Takeda 3A CMS at 25°C. The criteria of approximately 90% CH_4 purity with a relatively high CH_4 recovery are used to define the optimum run. Initially, the inlet feed velocity is changed to locate the optimum run without purge. Then the simulations were repeated around the optimum run to improve the PSA performance by introducing a purge and varying the durations of the individual steps in the PSA cycle. A purge gas of either 95% CH_4 or the product itself is used and the purge/feed ratio is adjusted to study their influence on separation.

From Table 5 the best performance (without purge) is given by Run no. 1, with the CH_4 product purity being closer to 90%. The countercurrent purge step is used to clean the adsorption bed. But for the CH_4/CO_2 separation on the Takeda

Table 4. Adsorption Bed Dimensions and Operating Conditions for Cycle (I) Used in PSA Simulation

Bed length	0.60 m
Diameter of adsorber bed	0.04 m
Bed external porosity	0.40
Bed density	695 kg/m^3
Feed composition	50% CO_2, 50% CH_4
Initial pressure	0.2 bar
Adsorption pressure (P_H)	4.0 bar
Desorption step end pressure	0.2 bar
Axial dispersion coefficient (D_{ax})	2.0×10^{-6} m^2/sec
Pressurization time	10 sec
Feed/adsorption time	60 sec
Blowdown time	10 sec
Desorption/purge time	60 sec

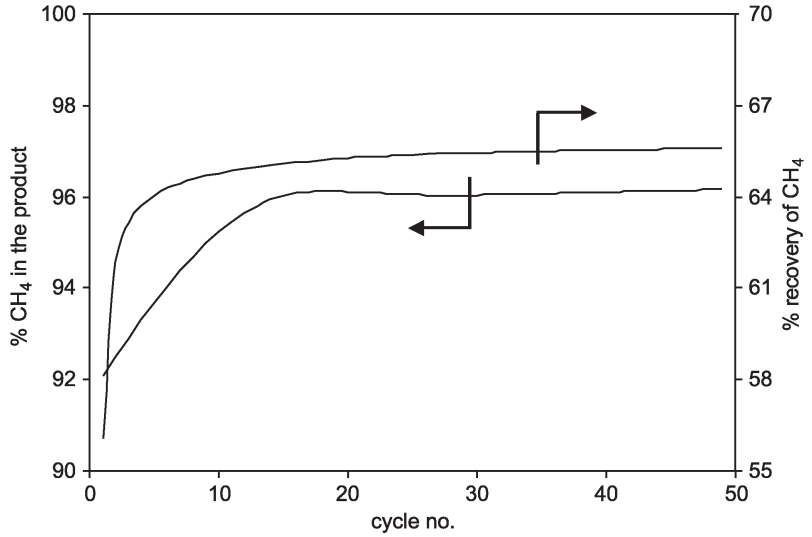

Figure 7. Theoretical steady-state approach of purity and recovery of CH_4 in PSA cycles.

Table 5. PSA Operating Parameters Used in the Simulation for CH_4/CO_2 Separation on Takeda 3A CMS at 25°C—Cycle (I) Described in Fig. 1

Run No.	Interstitial Feed Velocity (m/sec)	Purge/Feed Gas Ratio	Adsorption Product (CH_4) % Purity	Adsorption Product (CH_4) % Recovery	Productivity (kg CH_4/hr kg Sorbent)
1	0.015	—	87.2	20.9	0.0161
2	0.030	—	83.2	45.7	0.0481
3	0.40	—	80.6	55.9	0.0692
4	0.060	—	74.7	68.2	0.1100
5	0.080	—	69.7	75.1	0.1500
4[a]	0.060	—	71.4	74.8	0.1150
4[b]	0.060	—	68.8	78.8	0.1180
4[c]	0.060	—	77.6	54.0	0.0977
4[d]	0.060	0.237	76.0	68.3	0.1110
4(i)[d]	0.060	0.486	76.3	68.3	0.1110

[a] Adsorption and desorption step time of 90 sec.
[b] Adsorption and desorption step time of 120 sec.
[c] Adsorption and desorption step time of 30 sec.
[d] 95% CH_4 purge.

3A CMS, a purge stream of 95% CH_4 and a purge volume of 50% of feed improves the purity by only about 3%. This indicates that even excessive purge does not appreciably improve the product purity. The diffusivities of both CH_4 and CO_2 are low, hence for the adsorbed CO_2 to be evacuated the duration of the purge step needs to be sufficiently long. This increases the CH_4 recovery as shown by Runs 4^a, 4^b, and 4^c.

In the simple case of independent diffusion and isotherms the ratios of the uptakes is given by

$$\frac{K_A}{K_B}\sqrt{\frac{D_A}{D_B}}$$

in the linear range of the isotherms (6). For CH_4/CO_2 separation on Takeda molecular sieve, both equilibrium and kinetic selectivity are greater than unity and the ratios are found to increase with temperature. Hence, one of the possibilities to improve the performance of this kinetic PSA process is to increase the operating temperature. This makes the diffusion faster. However, the equilibrium adsorption would be decreased. Hence, the net effects of increasing the temperature on the working capacity of the sorbent and performance of the PSA separation needs to be examined in detail because the isotherms are nonlinear in this case.

The simulations are repeated for Takeda 3A at 70°C to study the net effects of temperature on the process performance. The increase in operating temperature increases the diffusion rates, but also decreases the capacity of the sorbent. From the simulation results tabulated in Table 6, we find that the recovery increases by almost 40% for the same purity level, while at the same time, the productivity is more than doubled due to the increased throughput. At 70°C, the introduction of a purge gas shows appreciable improvements in the product purity and productivity, but the recovery is decreased. The durations of the feed and desorption steps are changed in all combinations in order to study their effects on the separation performance. It is found that increase in adsorption step times gives marginally poor purity while better recovery and productivity.

The simulations on BF CMS for Cycle (I) are performed at 25°C and the results are given in Table 7. The best result of approximately 90% CH_4 purity with a recovery of 65% is obtained, which is comparable to the 65% CH_4 recovery obtained for Takeda 3A at 70°C. The effect of purge for BF CMS beds is appreciable with the productivity increasing significantly for a comparison made on equal product purity level. The comparison of the performance of the runs in Tables 5–7 is shown in Fig. 12 on a comparison scale of productivity. From Fig. 12(a), we see that the Takeda 3A CMS at a higher operating temperature of 70°C gives a better CH_4 purity than both BF and Takeda 3A CMS at 25°C. Figure 12(b) shows that the two sorbents, Takeda 3A and BF CMS, give the same product recovery with no dependence on temperature.

Table 6. PSA Operating Parameters Used in Simulation for CH_4/CO_2 Separation on Takeda 3A CMS at 70°C—Cycle (I) Described in Fig. 1

Run No.	Interstitial Feed Velocity (m/sec)	Purge/Feed Gas Ratio	Adsorption Product (CH_4) % Purity	Adsorption Product (CH_4) % Recovery	Productivity (kg CH_4/hr kg Sorbent)
1	0.015	—	98.8	18.8	0.0141
2	0.030	—	95.9	41.1	0.0407
3	0.040	—	94.5	50.6	0.0585
4	0.060	—	92.2	63.4	0.0940
5	0.080	—	90.1	71.7	0.1300
6	0.100	—	88.6	77.0	0.1650
7	0.120	—	86.0	81.0	0.2000
8	0.150	—	82.7	85.1	0.2520
6[a]	0.100	—	85.7	83.8	0.1750
6[b]	0.100	—	82.2	87.6	0.1800
6[c]	0.100	—	89.9	62.9	0.1430
6[d]	0.100	—	85.0	78.9	0.2130
6[e]	0.100	—	84.3	84.5	0.2070
6[f]	0.100	—	89.2	76.1	0.1350
6[g]	0.100	0.231	93.5	76.9	0.1660
6(i)[g]	0.100	0.537	96.8	76.7	0.1660
6[h]	0.100	0.231	93.5	53.8	0.1160

[a] Adsorption and desorption step time of 90 sec.
[b] Adsorption and desorption step time of 120 sec.
[c] Adsorption and desorption step time of 30 sec.
[d] Adsorption step time of 60 sec and desorption step time of 30 sec.
[e] Adsorption step time of 90 sec and desorption step time of 60 sec.
[f] Adsorption step time of 60 sec and desorption step time of 90 sec.
[g] 95% CH_4 purge.
[h] Product purge.

Cycle (II)

The PSA simulation results for Cycle (II) using Takeda 3A CMS at 25 and 70°C are given in Table 8, along with those for BF CMS at 25°C for a total cycle time of 240 sec. These simulation results give higher CH_4 purities and lower recoveries when compared with the experimental results of Kapoor and Yang (8). This is because the feed throughput is very high in the simulation compared to the experiments. The experiments on BF CMS yielded

Table 7. PSA Operating Parameters Used in the Simulation for CH_4/CO_2 Separation on BF CMS at 25°C—Cycle (I) Described in Fig. 1

Run No.	Interstitial Feed Velocity (m/sec)	Purge/Feed Gas Ratio	Adsorption Product (CH_4) % Purity	Adsorption Product (CH_4) % Recovery	Productivity (kg CH_4/hr kg Sorbent)
1	0.015	—	98.7	19.7	0.0167
2	0.030	—	94.5	43.0	0.0482
3	0.040	—	92.4	52.8	0.0690
4	0.060	—	88.9	66.0	0.1110
5	0.080	—	85.6	74.2	0.1520
6	0.100	—	82.4	79.5	0.1930
7	0.120	—	79.2	83.1	0.2340
6[a]	0.100	0.077	84.5	79.4	0.1930
6(i)[a]	0.100	0.448	91.8	78.7	0.1940
6[b]	0.100	0.077	84.5	71.7	0.1750

[a] 95% CH_4 purge.
[b] Product purge.

Table 8. PSA Operating Parameters Used in the Simulation for CH_4/CO_2 Separation Takeda 3A CMS at 25°C—Cycle (II) Described in Ref. (8)

Run No.	Adsorption Product Outlet Velocity (m/sec)	Pressure After Cocurrent Depressurization (bar)	Adsorption Product (CH_4) % Purity	Adsorption Product (CH_4) % Recovery	Productivity (kg CH_4/hr kg Sorbent)
Takeda 3A CMS at 25°C					
1	0.0025	3.36	93.5	14.7	0.00486
2	0.0085	2.60	85.8	39.2	0.0152
3	0.0170	1.29	78.9	59.1	0.0279
Takeda 3A CMS at 70°C					
4	0.0025	3.36	99.9	13.4	0.00451
5	0.0085	2.60	97.9	39.4	0.0150
6	0.0170	1.29	94.3	64.2	0.0290
Bergbau–Forschung CMS at 25°C					
7	0.0025	3.36	99.2	13.7	0.00516
8	0.0085	2.60	97.2	40.8	0.0172
9	0.0170	1.29	91.9	65.7	0.0325

more than 90% purity and recovery of CH_4 (8) when operated under Cycle (II) configuration.

Two main conclusions may be drawn from a comparison of Cycle (I) and Cycle (II). First, a high-pressure feed step is desirable, as the results are much better from Cycle (I). The reason for this conclusion is seen in the bed profiles, where it is seen that a high amount of CO_2 is adsorbed during the feed step. The second conclusion is that a low-pressure purge step is *not* desirable for the kinetics-based separation, unless a high purity product is the most desirable result (compared with recovery and productivity). The reason for this conclusion is also clear from the bed profiles. During the purge step, actually more methane is adsorbed than carbon dioxide.

Bed Concentration Profiles—Adsorber Dynamics

The analysis of concentration profiles in the bed gives better illustration of the mass transfer within the adsorption bed. Figure 8 shows the bed profiles at the end of each step in Cycle (I) at 25°C.

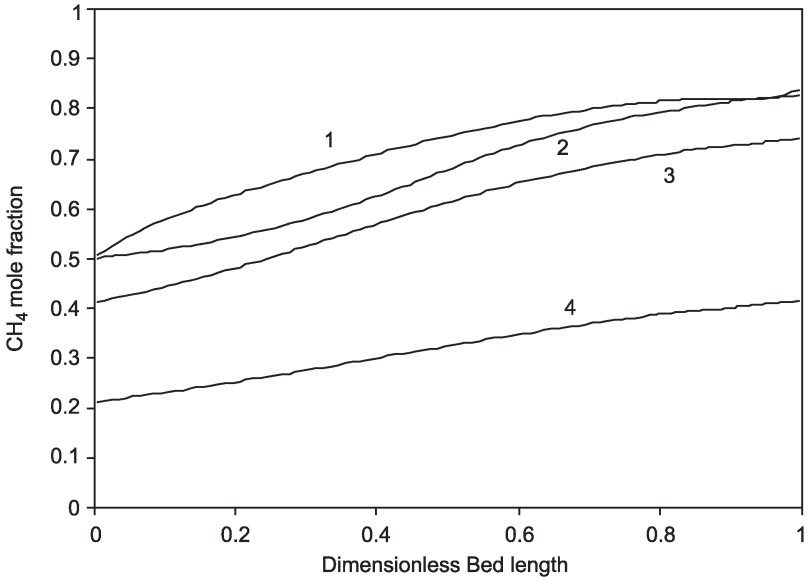

Figure 8. Concentration profile in the Takeda 3A CMS bed (25°C) at the end of each step (Run no. 4—Table 5): (1) pressurization; (2) feed/adsorption; (3) counter current blowdown; (4) counter current desorption.

The working capacity of the sorbent is quantitatively proportional to the area between the curves 2 and 4, i.e., at the ends of the adsorption and desorption steps. Therefore, this area may be defined as the sorbent working capacity for the specific PSA cycle. Figure 9 shows the bed profiles for the Takeda 3A CMS without purge at 70°C. The working capacity is higher at 70°C even though the total capacity of Takeda 3A is reduced by the higher temperature. This is due to the increase in diffusional time constants with temperature. The adsorption step [Step (2)] and blowdown step profiles [Step (3)] exhibit steeper concentration wavefronts. The steeper wavefronts lead to better separation results. The wavefronts are steeper for Takeda 3A at 70°C and BF CMS at 25°C. Figure 10 shows the Takeda 3A bed profiles at 70°C for the same conditions as in Fig. 9—with product purge. We find a slight decrease in the working capacity due to higher CH_4 concentration in the bed after purging with a product stream rich in CH_4, which results in a lower recovery of CH_4. The BF CMS bed profiles are shown in Fig. 11. In Fig. 11, the adsorption step profile [Step (2)] has started breaking through, which is not ideal for a separation process. The profiles are better for runs with CH_4

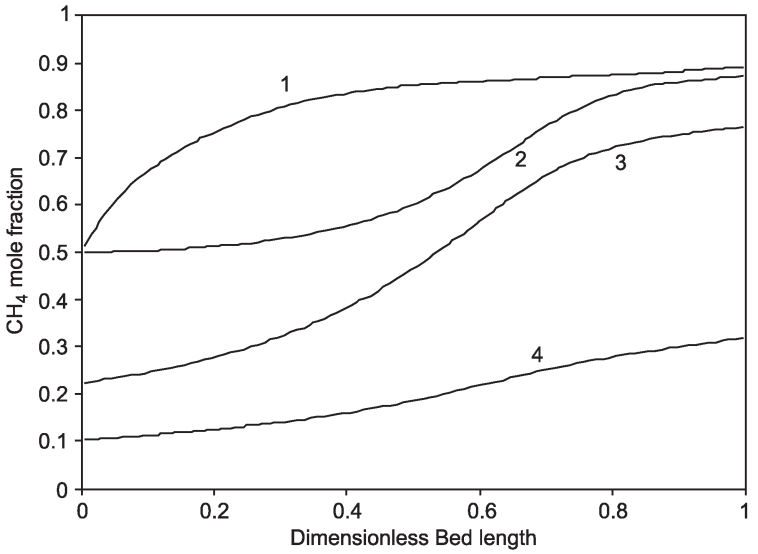

Figure 9. Concentration profiles in the Takeda 3A CMS bed (70°C) at the end of each step (Run no. 6—Table 6): (1) pressurization; (2) feed/adsorption; (3) counter current blowdown; (4) counter current desorption.

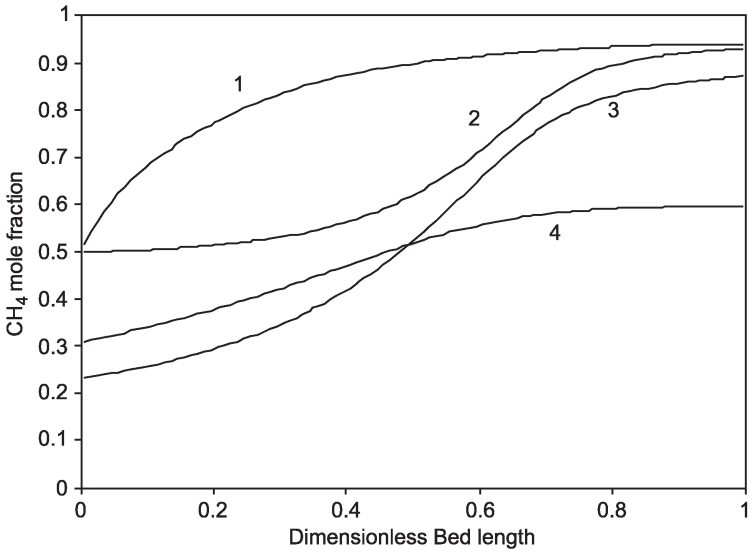

Figure 10. Concentration profiles in the Takeda 3A CMS bed (70°C) at the end of each step (Run no. 6^h—Table 6): (1) pressurization; (2) feed/adsorption; (3) counter current blowdown; (4) counter current purge with product.

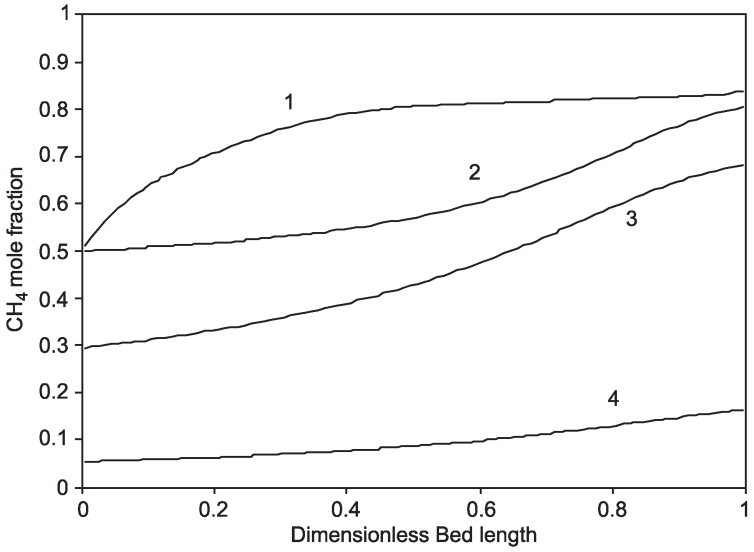

Figure 11. Concentration profiles in the BF CMS bed (25°C) at the end of each step (Run no. 6—Table 7): (1) pressurization; (2) feed/adsorption; (3) counter current blowdown; (4) counter current desorption.

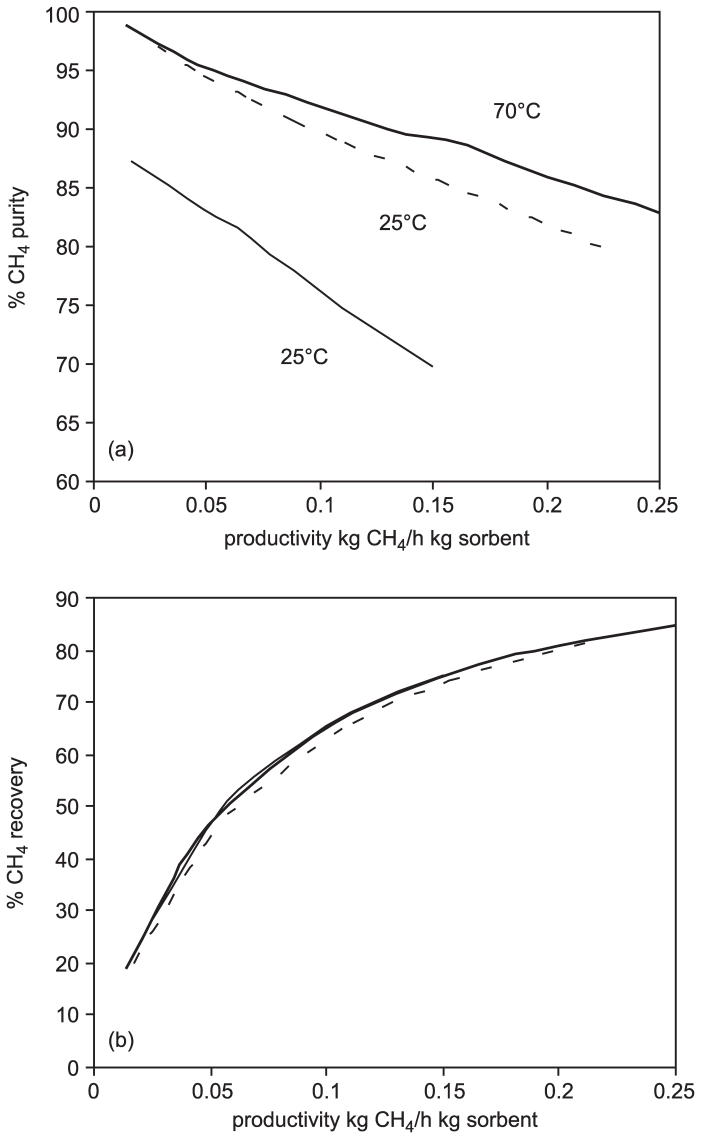

Figure 12. (a) CH_4 product purity (%) vs. productivity and (b) CH_4 recovery (%) vs. productivity for increasing feed velocities (operating conditions given in Table 5—Takeda 3A CMS at 25°C; Table 6—Takeda 3A CMS at 70°C; Table 7—BF CMS at 25°C). Solid line: Takeda 3A CMS; dashed line: BF CMS.

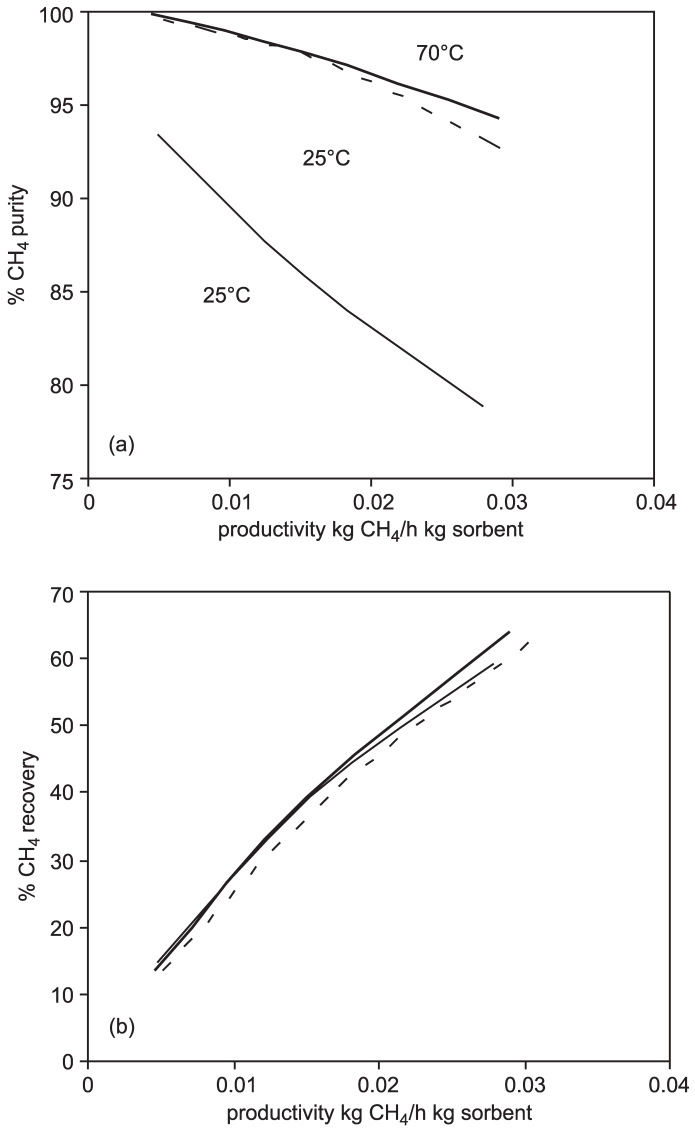

Figure 13. (a) CH_4 purity (%) vs. productivity and (b) CH_4 recovery (%) vs. productivity for increasing product velocities (operating conditions given in Table 8). Solid line: Takeda 3A CMS; dashed line: BF CMS.

purities higher than 90%. Figures 12 and 13 show the comparison of the two sorbents graphically for Cycle (I) and Cycle (II), respectively.

NOTATION

a_k	film resistance of component k (m/sec)
B	Langmuir parameter (atm^{-1})
D_{ax}	axial dispersion coefficient (m/sec^2)
D_e/r^2	diffusional time constant (sec^{-1})
L	length of the adsorption column (m)
P	pressure (bar)
P_{CBD}	pressure at the end of countercurrent blowdown step (bar)
P_{DES}	pressure at the end of desorption step (bar)
P_H	pressure in the adsorption step (bar)
q	adsorbed phase concentration (mmol/g)
q^*	equilibrium adsorbed phase concentration (mmol/g)
$\bar{q}$	average adsorbed phase concentration (mmol/g)
q_m	maximum adsorbed phase concentration (mmol/g)
R	radius of the spherical particle (m)
t	time (sec)
T	temperature (K)
u	gas phase velocity (m/sec)
z	axial position in the bed (m)
ε	bed porosity due to packing
ε_t	total bed porosity including macropores

REFERENCES

1. Boustany, K.; Narayanan, R.; Patton, C.J. Prism Separators. A Novel Process for Carbon Dioxide Removal from Hydrocarbon Gas, Rocky Mountain Regional Meeting of the Gas Processors Association, Denver, 1982.
2. Malik, V.A.; Lerner, S.L.; MacLean, D.L. Electricity, Methane and Liquid Carbon Dioxide Production from Landfill Gas, AIChE Spring National Meeting, Houston, Paper 47b, 1987.
3. Dreisbach, F.; Staudt, R.; Keller, J.U. High Pressure Adsorption Data of Methane, Nitrogen, Carbon Dioxide and Their Binary and Ternary Mixtures on Activated Carbon. Adsorption **1999**, *5*, 215–227.
4. Pereira, P.R.; Pires, J.; Brotas de Carvalho, M. Zirconium Pillared Clays for Carbon Dioxide/Methane Separation. 1. Preparation of Adsorbent Materials and Pure Gas Adsorption. Langmuir **1998**, *14*, 4584–4588.

5. Yang, R.T. *Gas Separation by Adsorption Processes*; [reprinted (in paper back) by Imperial College Press: London and World Scientific Publishing Co.: River Edge, NJ, 1997; 1–8] Butterworth: Boston, 1987.
6. Ruthven, D.M.; Farooq, S.; Knaebel, K.S. *Pressure Swing Adsorption*; VCH Publishers: New York, 1994; 1–10, 51–52, 230–232.
7. Rege, S.U.; Yang, R.T. Limits of Air Separation by Adsorption with LiX Zeolite. Ind. Eng. Chem. Res. **1997**, *36* (12), 5358–5365.
8. Kapoor, A.; Yang, R.T. Kinetic Separation of Methane–Carbon Dioxide Mixture by Adsorption on Molecular Sieve Carbon. Chem. Eng. Sci. **1989**, *44* (8), 1723–1733.
9. Ackley, M.W.; Yang, R.T. Diffusion in Ion-Exchanged Clinoptilolites. AIChE J. **1991**, *37* (11), 1645–1656.
10. Chen, Y.D.; Yang, R.T.; Uawithya, P. Diffusion of Oxygen, Nitrogen and Their Mixtures in Carbon Molecular Sieve. AIChE J. **1994**, *40* (4), 577–585.
11. Doong, S.J.; Yang, R.T. A Comparison of Gas Separation Performance by Different Pressure Swing Adsorption Cycles. Chem. Eng. Commun. **1987**, *54*, 61–71.
12. Kikkinides, E.S.; Yang, R.T.; Cho, S.H. Concentration and Recovery of CO_2 from Flue Gas by Pressure Swing Adsorption. Ind. Eng. Chem. Res. **1993**, *32* (11), 2714–2720.
13. Farooq, S.; Rathor, M.N.; Hidajat, K.A. A Predictive Model for a Kinetically Controlled Pressure Swing Adsorption Process. Chem. Eng. Sci. **1993**, *48*, 4129–4141.
14. Sun, L.M.; Le Quere, P.; LeVan, M.D. Numerical Simulation of Diffusion-Limited PSA Process Models by Finite Difference Methods. Chem. Eng. Sci. **1996**, *51* (24), 5341–5352.
15. Ma, Y.H.; Sun, W.; Bhandarkar, M.; Wang, J.; Miller, G.W. Adsorption and Diffusion of Nitrogen, Oxygen, Argon, and Methane in Molecular Sieve Carbon at Elevated Pressures. Sep. Purif. Technol. **1991**, *1*, 90–98.

Received May 2000
Revised November 2001